arXiv:2110.01334v2 [quant-ph] 2 Feb 2022

Enhanced TEMPO algorithm for quantum path integrals with off-diagonal system-bath coupling: applications to photonic quantum networks

Marten Richter[1,*] and Stephen Hughes[2]

[1] *Institut für Theoretische Physik, Nichtlineare Optik und Quantenelektronik, Technische Universität Berlin, Hardenbergstr. 36, EW 7-1, 10623 Berlin, Germany*
[2] *Department of Physics, Engineering Physics, and Astronomy, Queen's University, Kingston, Ontario K7L 3N6, Canada*

(Dated: February 3, 2022)

Multitime system correlations functions are relevant in various areas of physics and science, dealing with system-bath interaction including spectroscopy and quantum optics, where many of these schemes include an off-diagonal system bath interaction. Here we extend the enhanced TEMPO algorithm for quantum path integrals using tensor networks [Phys. Rev. Lett. 123, 240602 (2019)] to open quantum systems with off-diagonal coupling beyond a single two level system. We exemplify the approach on a coupled cavity waveguide system with spatially separated quantum two-state emitters, though many other applications in material science are possible, including entangled photon propagation, photosynthesis spectroscopy and on-chip quantum optics with realistic dissipation.

The theory of open quantum system remains a very active focus of current research [1–11], since it provides answers to many questions related to quantum computing, entanglement and communication, and also quantum networks. The theoretical frameworks include tensor network (TN) methods [10, 12–20] and quantum path integrals [2, 3, 5–11]. Recently these two approaches were successfully combined [9–11, 21], exploiting their combined advantages in the TEMPO (time-evolving matrix product operator) algorithm [9, 22] and an enhanced TEMPO (eTEMPO) algorithm [21]. Applications so far have mainly studied a two level system (TLS) *diagonally* coupled to an external bath [8–11, 21–23]. Beside these examples, many important problems remain to be studied in more detail, ranging from exciton relaxation in photosynthetic light harvesting systems [24–27] or nanostructures to exploit photon propagation, entanglement, superradiance and feedback [10, 19, 28–36]—which require *off-diagonal* system bath coupling. Mostly their treatment requires other algorithms such as hierarchical equations of motion [27, 37], and alternative TNs [10, 19].

Here we extend the eTEMPO method to include off-diagonal coupling as opposed to extending the TEMPO algorithm [38]. As input, we require only the generalized bath correlation function; in contrast to Ref. 39, where bath degrees of freedom are included and accessible in the network propagation, we show the effect of retardation for a two-cavity waveguide system on the first two rungs of photon transition. We demonstrate how the system transitions between one single generalized Jaynes-Cummings model (JCM) to a retardation regime between two JCMs, including a subradiant state. This manifests in a highly non-trivial non-Markovian dynamic, whose features *cannot* be captured with linearized response functions nor phenomenological JCMs.

Theoretically, a typical open quantum system, has system H_s and bath H_b Hamiltonian. Figure 1 shows an example integrated waveguide system, which is representative of emerging experiments with integrated semiconductor quantum dot systems [40–50]. The bath is harmonic, so Wick's theorem holds for factorizing initial conditions [51]. We consider a linear system bath interaction $H_{sb} = \sum_{ij\mu} C_{ij\mu} A_{ij} B_\mu$, where $C_{ij\mu}$ are the system-bath coupling constants, $A_{ij} = |i\rangle_s\langle j|_s$ (here in particular including $i \neq j$) and B_μ is a linear bath operator; for an harmonic bath $\mathrm{tr}(B_\mu \rho_B) = 0$. The dynamics of the full system-bath density matrix operator ρ obeys $\partial_t \rho = -\frac{i}{\hbar}(H_{s,-} + H_{b,-} + H_{sb,-})\rho$, where the subscripts $-, +, L, R$ convert a Hilbert space operator D to a Liouville space operator [24] with $D_L \rho = D\rho$ and $D_R \rho = \rho D$, and also $D_- = D_L - D_R$. Notably, the method can also include a Lindblad operators for system dynamics together with $H_{s,-}$. The time dynamics can be solved via the time ordered exponential $U(t,t_0) = T_{\leftarrow} \exp\left(-\frac{i}{\hbar}\int_{t_0}^{t} H_-(\tau)\mathrm{d}\tau\right)$ in Liouville space, $\rho(t) = U(t,t_0)\rho(t_0)$. Our observables of interest are multitime correlation functions $\langle T_{\leftarrow} A_1(t_1)\cdots A_N(t_N)\rangle$ with Liouville operators A_1, ...,A_N.

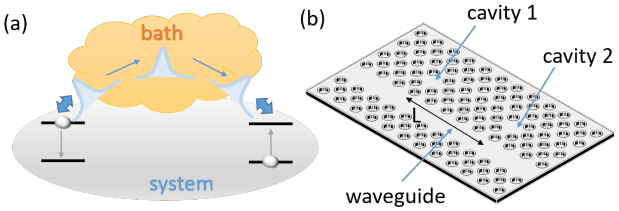


Figure 1. (a) Open quantum system coupled to a bath with excitation transfer through the bath. (b) Example system: photonic crystal with waveguide and two cavities separated by length L with a quantum emitter (TLS) in each cavity.

Next, we convert the correlation function into a quantum path integral formulation [2, 3, 5–11]; this allows us to develop an extended algorithm for systems with off-diagonal system-bath coupling, based on the

eTEMPO algorithm [21]—which is a very efficient algorithm for many quantum path integral TN implementations [9–11]. To proceed, we divide time t into intervals ΔT such that $t_n = n \cdot \Delta T$ with integer n. The times in the multitime correlation function should obey $t_i = \Delta T \cdot n_i$ with integer n_i, and we obtain $\langle T_{\leftarrow} A_1(t_1)...A_N(t_N)\rangle = \mathrm{tr}(O_M U_{M\text{-}1}...U_1 O_1 U_0 O_0 \rho(t_0))$, with $O_n = A_k$ if $t_k = \Delta T \cdot n$ for any k, otherwise $O_n = Id$; U_i is defined as $U_i = U(t_{i+1}, t_i)$. For most path integral implementations, the Suzuki-Trotter formula is applied to separate system and bath for the influence functional. We use perturbation theory and the Feynman disentanglement theorem. Perturbation theory to a limited order fails for processes involving many interactions over all times; thus, we apply perturbation theory to the individual intervals ΔT, so to U_i, keeping often only one system bath process per ΔT. For sufficient small ΔT, compared to system-bath coupling, a non-perturbative result is obtained with numerical accuracy. In general, $U_i = U_0(t_{i+1}, t_{i+\frac{1}{2}})\ U_I^{(i)}\ U_0(t_{i+\frac{1}{2}}, t_i)$, with $U_I^{(i)} = T_{\leftarrow} \exp\left(-\frac{i}{\hbar}\int_{t_i}^{t_{i+1}} U_0(t_{i+\frac{1}{2}}, \tau) H_{sb,-} U_0(\tau, t_{i+\frac{1}{2}}) \mathrm{d}\tau\right)$.

Restricting the system-bath coupling $H_{sb,-}$ to first order, per ΔT (and second order for non-vanishing bath correlation function, as explained after Eq. (3)), yields:

$$
\begin{aligned}
U_i &= U_0(t_{i+1}, t_{i+\frac{1}{2}}) U_{sb,i} U_0(t_{i+\frac{1}{2}}, t_i) \\
U_{sb,i} &= \Bigg(Id - \frac{i}{\hbar}\int_{t_i}^{t_{i+1}} \mathrm{d}\tau U_0(t_{i+\frac{1}{2}}, \tau) H_{sb,-} U_0(\tau, t_{i+\frac{1}{2}}) \\
&\quad - \frac{1}{\hbar^2}\int_{t_i}^{t_{i+1}} \mathrm{d}\tau_1 \int_{t_i}^{\tau_1} \mathrm{d}\tau_2 U_0(t_{i+\frac{1}{2}}, \tau_1) H_{sb,-} U_0(\tau_1, \tau_2) \\
&\qquad H_{sb,-} U_0(\tau_2, t_{i+\frac{1}{2}}) \Bigg), \qquad (1)
\end{aligned}
$$

with the time evolution operator $U_0(\cdot,\cdot)$ containing solely $H_{s,-}$ and $H_{b,-}$. The symmetric expansion with $U_0(\cdot,\cdot)$ on the left and right allows to exclude (include) certain parts of the Hamiltonian (e.g. like external optical excitation) in the inner brackets. Including second-order contributions from the same ΔT (cf. cumulant expansions [52]) prevents an artificial minimum delay between system bath interactions and reducing ΔT dependency, and thus recovers simple perturbation theory for weak coupling. We define $U_{0,i+\frac{1}{2}}^{\frac{1}{2}} = U_0(t_{i+\frac{1}{2}}, t_i)$ and rewrite $U_{sb,i} = U_{sb,i}^{(0)} + U_{sb,i}^{(1)} + U_{sb,i}^{(2)}$, with the k-th order system-bath contribution $U_{sb,i}^{(k)}$; $H_{sb,-}$ contains system A and bath operators B, so we apply $(AB)_- = A_+ B_- + A_- B_+$. Finally, $U_{sb,i}^{(k)}$ can be written as $U_{sb,i}^{(k)} = \sum_l A_l^{(k)} B_l^{(k)}$ with Liouville system operators $A_l^{(k)}$ and bath operators $B_l^{(k)}$(each with a maximum k linear bath operators).

With an initial factorizing density matrix $\rho(t_0) = \rho_s \otimes \rho_b$, then

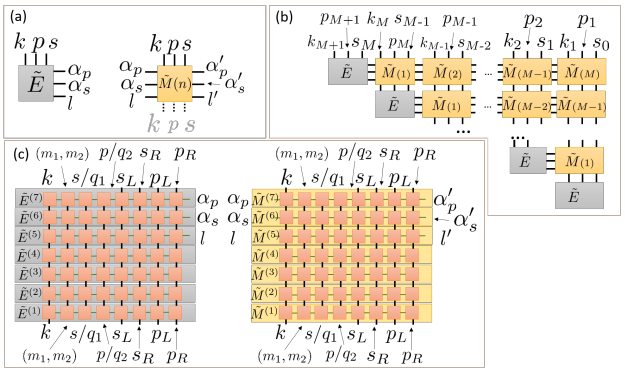


Figure 2. (a) Tensors $\tilde{E}$ and $\tilde{M}$ depicted as rectangle and indices. (b) TN for the influence functional from Eq. (4), c) decomposition of the $\tilde{E}$ and $\tilde{M}$ into seven matrix product operators (indices are connected with delta tensors).

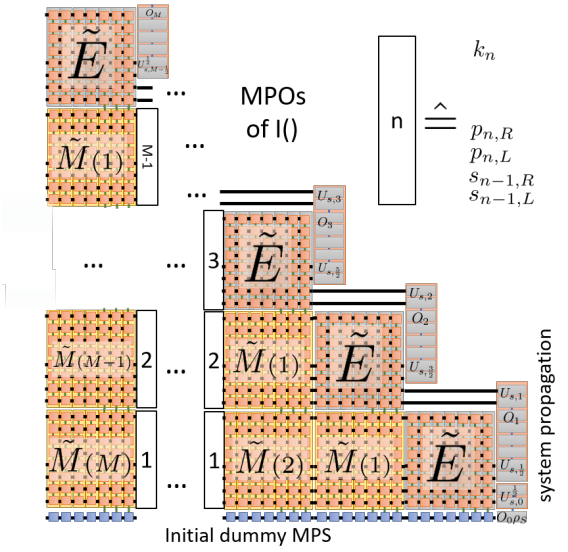


Figure 3. TN for $\langle T_{\leftarrow} A_1(t_1)...A_N(t_N)\rangle$. On the right edge of the TN the MPS decomposed system propagators $U_{s,m-1/2}$ (cf. Eq.(2)) are connected to the indices s and p. The majority of network is constructed from the decomposed $\tilde{M}$ and $\tilde{E}$ tensors. An initial MPS is at the bottom.

$$
\begin{aligned}
&\langle T_{\leftarrow} A_1(t_1) \cdots A_N(t_N)\rangle = \qquad (2) \\
&\sum_{k_{M-1}...k_0=0}^{2} \sum_{l_{M-1}...l_0} \mathrm{tr}_b(U_{b,M-\frac{1}{2}} B_{l_{M-1}}^{(k_{M-1})} \ldots U_{b,\frac{1}{2}} B_{l_0}^{(k_0)} \rho_B) \\
&\cdot \mathrm{tr}_s(O_M U_{s,M-\frac{1}{2}} A_{l_{M-1}}^{(k_{M-1})} \ldots O_1 U_{s,\frac{1}{2}} A_{l_0}^{(k_0)} U_{s,0}^{\frac{1}{2}} O_0 \rho_S),
\end{aligned}
$$

holds with the bath $U_{b,i}$ and system $U_{s,i}$ time propagation. For initial thermal correlated $\rho(t_0)$, a Liouville operator A_c can be included in O_0 [53], while keeping an harmonic ρ_B in Eq. (2).

To convert the expressions to a quantum path integral, we insert Liouville space iden-

tities: $Id = \sum_{s_L,s_R}(|s_L\rangle\langle s_L|)_L(|s_R\rangle\langle s_R|)_R$, using a H_s eigenbasis. Using the notation $A = \sum_{s,p} A^{p_L s_L}_{p_R s_R}(|p_L\rangle\langle s_L|)_L(|s_R\rangle\langle p_R|)_R$ for expanding any operator A, we obtain $\langle T_{\leftarrow} A_1(t_1)\cdots A_N(t_N)\rangle = \sum_{\{k\}\{s\}\{p\}} I(s_0,p_1,s_1,...,p_M,s_M)\mathrm{tr}_s\left[\tilde{O}_{s_M p_M}..\tilde{O}_{s_1 p_1}\tilde{\rho}_{s_0 p_0}\right]$, with the convention $\{x\} = x_1 \dots x_M$ for indices and with $\tilde{O}_{s_n p_n} = \left(O_n U_{s,n-1/2}\right)_{s_n p_n}$ and $\tilde{\rho}_{s_0 p_0} = \left(U^{\frac{1}{2}}_{s,0} O_0 \rho_S\right)_{s_0 p_0}$. Without subscripts L or R, an index includes left and right Liouville space. We replace the index l and the operators $A^{(k)}_l$ with indices s and p, and an according redefinition of operator matrix elements $B^{(p_j s_j)}_{k_j}$ including the free bath propagation (and indicating the interval with index j) in the influence functional I, so that $I(s_0,p_1,k_1,\dots,p_M,s_M,k_M) = \mathrm{tr}_B(B^{(p_M s_{M-1})}_{k_{M-1}}\dots B^{(p_2 s_1)}_{k_1} B^{(p_1 s_0)}_{k_0}\rho_b)$.

Wick's theorem holds for factorization, since the harmonic bath is initially in thermal equilibrium (no photons). Thus, I factorizes into expectation values of two linear bath operators, with each linear bath operator from a different interval ΔT or two from the same interval ΔT. We arrive at an iterative expression for I:

$$
\begin{aligned}
&I(s_0,p_1,k_1) = E_{s_0 p_1 k_1}, \qquad (3)\\
&I(s_0,p_1,k_1,...,s_M,p_{M+1},k_{M+1})\\
&\quad = E_{s_M,p_{M+1},k_{M+1}} I(s_0,p_1,k_1,...,s_{M-1},p_M,k_M)\\
&\qquad + \delta_{k_{M+1},1}\sum_{m=1}^{M}\delta_{k_m,1} M^{p_{m+1}s_m}_{s_M,p_{M+1},k_{M+1}}\\
&\qquad\quad \cdot I(s_0,p_1,k_1,...,s_{m-1},p_m,-1,...,s_{M-1},p_M,k_M),
\end{aligned}
$$

where $E_{s,p,k}$ describes the current time interval with zero (δ_{sp}), two ($B^{(ps)}_2$) or one system-bath interactions, and $k=-1$ is added to link to previous times: $E_{s,p,k} = (\delta_{sp}\delta_{k,0} + \delta_{k,2}\mathrm{tr}_b(B^{(ps)}_2\rho_B) + \delta_{k_1,-1})$. Here $M^{p_{m+1}s_m}_{s_M,p_{M+1},k_{M+1}}$ describes a process, with one interaction in the interval m (e.g., photon emission) and one in the interval $M+1$ (e.g., photon absorption): $M^{p_{m+1}s_m}_{s_M,p_{M+1},k_{M+1}} = \delta_{k_{M+1},1}\mathrm{tr}_b(B^{(s_M,p_{M+1})}_1 B^{(s_m,p_{m+1})}_1\rho_b)$, and depends only on the time difference $M-m$ for time independent bath Hamiltonians.

Note that $M^{p_{m+1}s_m}_{s_M,p_{M+1},k_{M+1}}$ contains a generalized bath correlation function, directly connected to a generalized spectral density for off-diagonal coupling [24], which fully determines the system bath-interaction. The tensor M describes a boson going into the bath at m and back to the system at $M+1$. We discuss differences to the quantum path integrals with diagonal coupling—the standard influence functional [2, 3, 5–11, 21]. For the common case, the I depends only on one index s per ΔT, where for the off-diagonal case it depends on initial s and final p index and the k the number of system bath interactions per ΔT. We note, hitherto, most numerically exact treatments with TN focused only on diagonal coupling.

We reformulate Eq. (3) for easier conversion to a TN:

$$
\begin{aligned}
&I(s_0,p_1,k_1,...,s_M,p_{M+1},k_{M+1}) =\\
&\sum_{\{k'\}\{l\}\{\alpha_p\}\{\alpha_s\}}\prod_{m=1}^{M}\tilde{E}^{\alpha_{p_M}\alpha_{s_M} l}_{s_M p_{M+1} k_{M+1}}\cdot\tilde{M}^{k'_m\alpha_{p_{m-1}}\alpha_{s_{m-1}}l_{m-1}}_{p_{m+1}s_m k_m\alpha_{p_m}\alpha_{s_m}l_m}(n)\cdot\\
&\qquad I(s_0,p_1,k'_1,...,s_{M-1},p_M,k'_M)\cdot\delta_{\alpha_{p_1}1}\delta_{\alpha_{s_0}1}\delta_{l_1 1}, \qquad (4)
\end{aligned}
$$

with modified tensors $\tilde{M}$ and $n = M+1-m$:

$$
\begin{aligned}
\tilde{M}^{k'\alpha'_p\alpha'_s l'}_{psk\alpha_p\alpha_s l}(n) =&\delta_{k,1}\delta_{k',-1}\delta_{\alpha'_p,1}\delta_{\alpha'_s,1}\delta_{l_m,1}G_{psl\alpha_p-1\alpha_s-1}(n)\\
&+\delta_{k,k'}\delta_{\alpha_p\alpha'_p}\delta_{\alpha_s\alpha'_s}\delta_{ll'}, \qquad (5)
\end{aligned}
$$

where $G(n)$ is the double integrated system bath correlation function (Eq. (1)) between two ΔT intervals, which are $n\Delta T$ apart. The first interaction acts on left (right) side in Liouville space for $l=1$ ($l=2$) respectively, changing the left/right state from $\alpha_s - 1$ to $\alpha_p - 1$. $\alpha'_{p/s} = 1$ encodes no further interaction in subsequent ΔT. In Eq. (5) the modified tensor $\tilde{E}$ appears:

$$
\begin{aligned}
\tilde{E}^{\alpha_p,\alpha_s l}_{s,p,k} =& \big[\delta_{k,0}\delta_{sp} + \delta_{k,2}G_{ps} + \delta_{k,-1} \qquad (6)\\
&+\delta_{k,1}(\delta_{l,1}\delta_{\alpha_p,p_L+1}\delta_{\alpha_s,s_L+1} + \delta_{l,2}\delta_{\alpha_p,p_R+1}\delta_{\alpha_s,s_R+1})\big]
\end{aligned}
$$

where the C tensor contains the system-bath correlation within the first interval ΔT.

Equation (4) is now converted to a TN, where we depict a tensor as, e.g., T_{ijk} as a rectangle and each index i,j,k as a line (cf. Fig. 2a)), where connected indices between tensors indicate a summation [13]. The TN depicted in Fig. 2(b), built up from tensors $\tilde{E}$ and $\tilde{M}$, can be contracted by interpreting the first row as a matrix product state (MPS) and the subsequent rows as matrix product operator (MPO), and applying MPOs to MPS subsequently [13]. The TN is the TEMPO [9] implementation for the off-diagonal case.

Because of the increased tensor rank in the off-diagonal case, the TEMPO algorithm is highly ineffective especially beyond a single TLS. Here we construct a TN that reduces the index dimension and yields the original tensors after contraction. Therefore, we design a product of 6 (and 7) low rank and low dimensional tensors that yield $\tilde{M}^{(\cdot)}$ (and $\tilde{E}$). These are also decomposed into a MPS [54] and the resulting MPSs are connected via δ-tensors to obtain the TN of MPOs in Fig. 2(c). Further details are given in the Supplemental Information [55].

Following the idea from Ref. 21, that the indices on $\tilde{E}$ can be moved to the other edge of the network from Fig. 2(b) (rotating the TN by ninety degrees), we obtain the decomposed TN as in Fig. 3. Then the TN (Fig. 3), including the temporal propagation of the system from Eq. (4), is contracted to obtain the expectation values. For evaluation, the MPOs are applied row by row (Fig. 4 (i)-(iii), Eq. (3) using *exactapply* from itensor [56]), thus implementing the eTEMPO algorithm [21]

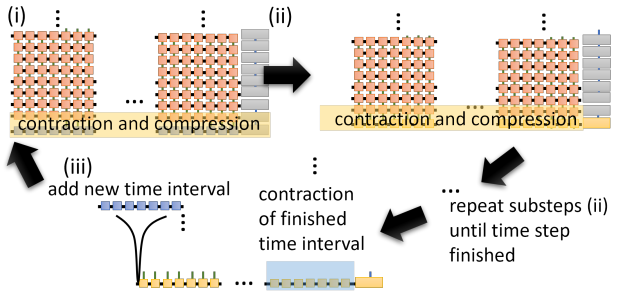


Figure 4. (i) Application of next MPO to the current MPS (initially a dummy MPS) (ii) repeated until all tensors of ΔT are contracted, then (iii) removal of the current interval, and extension for future intervals. (i) Repeated, until finished.

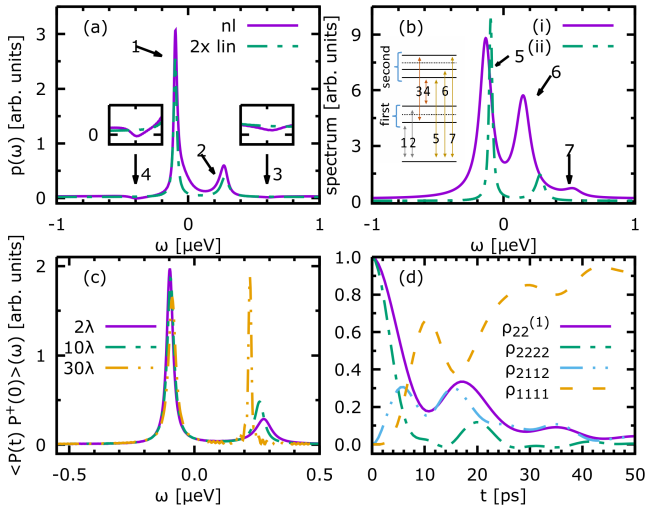


Figure 5. (a) Nonlinear (nl) and linear (lin) spectra for the setup from Fig. 1b) with a TLS resonant to both cavity frequencies. (b) Fourier transform of (i) double $\langle P(t)P(t)P^\dagger(0)P^\dagger(0)\rangle$ and (ii) single quantum $\langle P(t)P^\dagger(0)\rangle$ emitter polarisation correlation function with $P^\dagger = \sum_l \mathbf{d}|2\rangle_l\langle 1|_l$ (inset JCM Ladder). (c) Single quantum from (b) for different L. (d) Time dynamics of the upper level of reduced density matrix $\rho_{22}^{(1)}$ of one emitter, and for both emitters ρ_{nmmn} when both are initially excited.

variant for the offdiagonal case in itensor (version 2.1.0 patched) [56]. Tensors in the MPS connected to previous times are traced out, achieving a massive reduction of computational time (cf. Fig. 4). Then a row of blocks in the network are added to the current MPS to extend the covered time, if required.

Critically, our framework is capable of including both diagonal and off-diagonal coupling and is thus applicable to a multitude of problems, including exciton-phonon dynamics in (coupled) nanostructures [7, 57–61], photosynthetic pigment-protein complex [25, 26, 62], as well as quantum optics system including plasmonics [10, 28–32, 63, 64]. To demonstrate the power of our approach, we consider *a quantum network example, with on-chip photonic propagation*, fully consistent with a rigorous Maxwell solution theory of a photonic crystal with a waveguide and two integrated cavities [65] as depicted in Fig. 1(b) (system parameters in [55]). This scheme is also timely with recent experiments [66].

We assume a TLS with $H_s = \sum_{li} \epsilon_{i_l} |i\rangle_l\langle i|_l$, in each cavity, where ϵ_{i_l} is the energy of level i in system l. The photonic crystal medium can be quantized using the Green's function $\mathbf{G}(\mathbf{r},\mathbf{r}',\omega)$ of the Helmholtz equation [55, 65, 67]. The electric field operator is $\mathbf{E}(\mathbf{r},\omega) = i\sqrt{\frac{\hbar}{\pi\epsilon_0}} \int \mathrm{d}^3r' \sqrt{\epsilon_I(\mathbf{r}',\omega)}\mathbf{G}(\mathbf{r},\mathbf{r}',\omega)\cdot\mathbf{b}(\mathbf{r}',\omega)$, where $\mathbf{b}(\mathbf{r},\omega)$ are boson operators that form the bath for the path integral approach: $H_B = \hbar \int \mathrm{d}^3r \int_0^\infty \mathrm{d}\omega\, \omega \mathbf{b}^\dagger(\mathbf{r},\omega)\cdot\mathbf{b}(\mathbf{r},\omega)$. A dipole coupling $\mathbf{d}_{ij}^{(i)}$ for the i emitter at position $\mathbf{r}_i$ to the bath constitutes the system-bath interaction $H_{sb} = \sum_{nij} |i\rangle_n\langle j|_n \mathbf{d}_{ij}^{(n)} \cdot \int_0^\infty \mathrm{d}\omega \mathbf{E}(\mathbf{r}_n,\omega) + \text{H.a.}$. The correlation function $C_{ijkl}^{nm}(\tau) = \frac{1}{\hbar\pi\epsilon_0} \int \mathrm{d}\omega e^{-i\omega\tau} \mathbf{d}_{ij}^{(n)} \cdot \mathrm{Im}(G(\mathbf{r}_n,\mathbf{r}_m,\omega)) \cdot \mathbf{d}_{kl}^{*(m)}$ characterizes the system-bath coupling and dynamics and therefore is also present in the decomposed tensors G [55] via $G_{ijkl}^{nm(\tilde{i})} = -\int_{t_{\tilde{i}}}^{t_{\tilde{i}+1}} \mathrm{d}\tau_1 \int_{t_{\tilde{i}}}^{\tau} \mathrm{d}\tau_1 e^{i((\epsilon_i-\epsilon_j)\tau_2+(\epsilon_k-\epsilon_l)\tau_1} C_{ijkl}^{nm}(\tau_2 - \tau_1)$ and $G_{ijkl}^{nm(\tilde{i}\tilde{j})} = -\int_{t_{\tilde{i}}}^{t_{\tilde{i}+1}} \mathrm{d}\tau_1 \int_{t_{\tilde{j}}}^{t_{\tilde{j}+1}} \mathrm{d}\tau_1 e^{i(\epsilon_i-\epsilon_j)\tau_2+i(\epsilon_k-\epsilon_l)\tau_1)} C_{ijkl}^{nm}(\tau_2 - \tau_1)$.

For our example system shown in Fig. 1(b), the TLSs are chosen resonant with the cavity modes. We excite the TLSs by a few-fs pulse described by $H_{\text{ext}} = \sum_l \mathbf{d}\cdot\mathbf{E}(t)e^{i\omega_l t}|2\rangle_l\langle 1|_l + \text{H.a.}$. The pulse does not excite the photons directly. A Fourier transform of the TLS polarization is shown in Fig. 5(a). [68] The low intensity plot (linear spectrum) shows modified Rabi splitting between peaks 1 and 2 (cf. Ref. 65) and the upper state (2) shows a lifetime broadening due to a transfer process to a lower state (e.g. state 1). A longer delay (increasing L, with the same phase) between the TLS affects the upper state, caused by inter cavity transfer of photons. So the long inter cavity delay turns the upper state to a sub radiant state with reduced broadening. Thus, the two cavities do not act as a single effective JCM model anymore; this is also true for the upper state in the higher rungs of the JCM ladder, which we study below.

For nonlinear excitation, shown also in Fig. 5(a) (0.45π, half excited), we observe additional (negative) peaks 3 and 4. A comparison to the energies in the single and double quantum function, in Fig. 5(b),indicates that these match well with transitions between the first and second rung of the JCM ladder. The single and double quantum function give the coherences of a system between ground state and single or double excitation states (respectively) [69–72] and allows a direct inspection of their energies (see [55] for more details on our quantum correlation functions). Other (positive) contributions between the first and second rung are overlapping

with resonances 1 and 2, which slightly affect their line shape. The negative peaks 3 and 4 appear only in our nonlinear solution, showing complex interference effects beyond weak excitation. Although the origin of such line shapes are hard to identify, they may be related to an excitation transfer process [55]. The time dynamics of densities in Fig. 5(d) shows the typical Rabi oscillations. Furthermore correlations between the two TLS densities (Fig. 5(d)), allow access to complex entanglement properties.

We highlight that for many example systems, the bath correlation time is longer than the simulation time—a notoriously difficult test for the numerical complexity without augmenting the density matrix [7], yielding simulation times of days or weeks depending on the bath correlation time and excitation. Overall the example demonstrates the potential for eTEMPO algorithms where off-diagonal coupling is important to include.

In summary, we have provided a generalized version of the eTEMPO algorithm [21] to include off-diagonal system bath coupling, opening the route for numerically exact treatment of off-diagonal system bath coupling in exciton migration (e.g. coupled nanostructures, photosynthesis) or quantum light propagation in plasmonics and photonic networks. In particular, we have shown how delay and round trip coherence alters the JCM like behavior.

Acknowledgments—We acknowledge funding from Queen's University, the Canadian Foundation for Innovation, the Natural Sciences and Engineering Research Council of Canada, and support from the Alexander von Humboldt Foundation through a Humboldt Research Award.

* marten.richter@tu-berlin.de

[1] H.-P. Breuer, F. Petruccione, *et al.*, *The theory of open quantum systems* (Oxford University Press on Demand, 2002).

[2] A. Caldeira and A. Leggett, Path integral approach to quantum brownian motion, Physica A **121**, 587 (1983).

[3] Y. Tanimura and S. Mukamel, Real-time path-integral approach to quantum coherence and dephasing in nonadiabatic transitions and nonlinear optical response, Phys. Rev. E **47**, 118 (1993).

[4] M. Richter and A. Knorr, A time convolution less density matrix approach to the nonlinear optical response of a coupled system-bath complex, Annals of Physics **325**, 711 (2010).

[5] N. Makri and D. E. Makarov, Tensor propagator for iterative quantum time evolution of reduced density matrices. i. theory, J. Chem. Phys. **102**, 4600 (1995).

[6] N. Makri and D. E. Makarov, Tensor propagator for iterative quantum time evolution of reduced density matrices. ii. numerical methodology, J. Chem. Phys. **102**, 4611 (1995).

[7] A. Vagov, M. D. Croitoru, M. Glässl, V. M. Axt, and T. Kuhn, Real-time path integrals for quantum dots: Quantum dissipative dynamics with superohmic environment coupling, Phys. Rev. B **83**, 094303 (2011).

[8] A. Strathearn, B. W. Lovett, and P. Kirton, Efficient real-time path integrals for non-markovian spin-boson models, New Journal of Physics **19**, 093009 (2017).

[9] A. Strathearn, P. Kirton, D. Kilda, J. Keeling, and B. W. Lovett, Efficient non-markovian quantum dynamics using time-evolving matrix product operators, Nature communications **9**, 3322 (2018).

[10] O. Kaestle, R. Finsterhoelzl, A. Knorr, and A. Carmele, Continuous and time-discrete non-markovian system-reservoir interactions: Dissipative coherent quantum feedback in liouville space, Phys. Rev. Research **3**, 023168 (2021).

[11] E. V. Denning, M. Bundgaard-Nielsen, and J. Mørk, Optical signatures of electron-phonon decoupling due to strong light-matter interactions, Phys. Rev. B **102**, 235303 (2020).

[12] R. Orús, A practical introduction to tensor networks: Matrix product states and projected entangled pair states, Annals of Physics **349**, 117 (2014).

[13] U. Schollwöck, The density-matrix renormalization group in the age of matrix product states, Annals of physics **326**, 96 (2011).

[14] J. Cirac, D. Pérez-García, N. Schuch, and F. Verstraete, Matrix product density operators: Renormalization fixed points and boundary theories, Annals of Physics **378**, 100 (2017).

[15] F. Verstraete and J. I. Cirac, Matrix product states represent ground states faithfully, Physical Review B **73**, 094423 (2006).

[16] G. Vidal, Classical simulation of infinite-size quantum lattice systems in one spatial dimension, Physical review letters **98**, 070201 (2007).

[17] S. R. Clark, J. Prior, M. J. Hartmann, D. Jaksch, and M. B. Plenio, Exact matrix product solutions in the Heisenberg picture of an open quantum spin chain, New Journal of Physics **12**, 025005 (2010).

[18] A. H. Werner, D. Jaschke, P. Silvi, M. Kliesch, T. Calarco, J. Eisert, and S. Montangero, Positive tensor network approach for simulating open quantum many-body systems, Phys. Rev. Lett. **116**, 237201 (2016).

[19] H. Pichler and P. Zoller, Photonic circuits with time delays and quantum feedback, Phys. Rev. Lett. **116**, 093601 (2016).

[20] F. A. Schröder, D. H. Turban, A. J. Musser, N. D. Hine, and A. W. Chin, Tensor network simulation of multi-environmental open quantum dynamics via machine learning and entanglement renormalisation, Nature communications **10**, 1 (2019).

[21] M. R. Jørgensen and F. A. Pollock, Exploiting the causal tensor network structure of quantum processes to efficiently simulate non-markovian path integrals, Phys. Rev. Lett. **123**, 240602 (2019).

[22] A. Strathearn, *Modelling Non-Markovian Quantum Systems Using Tensor Networks* (Springer Nature, 2020).

[23] J. Kabuss, A. Carmele, M. Richter, W. W. Chow, and A. Knorr, Inductive equation of motion approach for a semiconductor qd-qed: Coherence induced control of photon statistics, physica status solidi (b) **248**, 872 (2011), https://onlinelibrary.wiley.com/doi/pdf/10.1002/pssb.201000851.

[24] V. Chernyak and S. Mukamel, Collective coor-

dinates for nuclear spectral densities in energy transfer and femtosecond spectroscopy of molecular aggregates, J. Chem. Phys. **105**, 4565 (1996), https://doi.org/10.1063/1.472302.

[25] W. M. Zhang, T. Meier, V. Chernyak, and S. Mukamel, Exciton-migration and three-pulse femtosecond optical spectroscopies of photosynthetic antenna complexes, J. Chem. Phys. **108**, 7763 (1998).

[26] G. Panitchayangkoon, D. Hayes, K. A. Fransted, J. R. Caram, E. Harel, J. Wen, R. E. Blankenship, and G. S. Engel, Long-lived quantum coherence in photosynthetic complexes at physiological temperature, Proceedings of the National Academy of Sciences **107**, 12766 (2010).

[27] T. Kramer, M. Noack, J. R. Reimers, A. Reinefeld, M. Rodriguez, and S. Yin, Energy flow in the photosystem i supercomplex: comparison of approximative theories with dm-heom, Chemical Physics **515**, 262 (2018).

[28] R. F. Oulton, V. J. Sorger, D. Genov, D. Pile, and X. Zhang, A hybrid plasmonic waveguide for subwavelength confinement and long-range propagation, Nature Photonics **2**, 496 (2008).

[29] M. I. Stockman, Nanofocusing of optical energy in tapered plasmonic waveguides, Physical review letters **93**, 137404 (2004).

[30] A. Orieux, M. A. Versteegh, K. D. Jöns, and S. Ducci, Semiconductor devices for entangled photon pair generation: a review, Reports on Progress in Physics **80**, 076001 (2017).

[31] M. Weiß and H. J. Krenner, Interfacing quantum emitters with propagating surface acoustic waves, Journal of Physics D: Applied Physics **51**, 373001 (2018).

[32] H. Jayakumar, A. Predojević, T. Kauten, T. Huber, G. S. Solomon, and G. Weihs, Time-bin entangled photons from a quantum dot, Nature communications **5**, 1 (2014).

[33] A. Carmele and S. Reitzenstein, Non-markovian features in semiconductor quantum optics: quantifying the role of phonons in experiment and theory, Nanophotonics **8**, 655 (2019).

[34] M. Richter and S. Mukamel, Collective two-particle resonances induced by photon entanglement, Phys. Rev. A **83**, 063805 (2011).

[35] M. Gegg, A. Carmele, A. Knorr, and M. Richter, Superradiant to subradiant phase transition in the open system dicke model: dark state cascades, New Journal of Physics **20**, 013006 (2018).

[36] S. Arranz Regidor, G. Crowder, H. Carmichael, and S. Hughes, Modeling quantum light-matter interactions in waveguide qed with retardation, nonlinear interactions, and a time-delayed feedback: Matrix product states versus a space-discretized waveguide model, Phys. Rev. Research **3**, 023030 (2021).

[37] Y. Tanimura and R. Kubo, Time evolution of a quantum system in contact with a nearly gaussian-markoffian noise bath, Journal of the Physical Society of Japan , 101–114https://doi.org/10.1143/JPSJ.58.101.

[38] D. Gribben, D. M. Rouse, J. Iles-Smith, A. Strathearn, H. Maguire, P. Kirton, A. Nazir, E. M. Gauger, and B. W. Lovett, Exact dynamics of non-additive environments in non-Markovian open quantum systems (2021), arXiv:2109.08442 [quant-ph].

[39] M. Cygorek, M. Cosacchi, A. Vagov, V. M. Axt, B. W. Lovett, J. Keeling, and E. M. Gauger, Numerically-exact simulations of arbitrary open quantum systems using automated compression of environments, arXiv preprint arXiv:2101.01653 (2021).

[40] F. Liu, A. J. Brash, J. O'Hara, L. M. P. P. Martins, C. L. Phillips, R. J. Coles, B. Royall, E. Clarke, C. Bentham, N. Prtljaga, I. E. Itskevich, L. R. Wilson, M. S. Skolnick, and A. M. Fox, High Purcell factor generation of indistinguishable on-chip single photons, Nature Nanotechnology **13**, 835 (2018).

[41] C. P. Dietrich, A. Fiore, M. G. Thompson, M. Kamp, and S. Höfling, GaAs integrated quantum photonics: Towards compact and multi-functional quantum photonic integrated circuits, Laser & Photonics Reviews **10**, 870 (2016).

[42] R. Bose, D. Sridharan, H. Kim, G. S. Solomon, and E. Waks, Low-photon-number optical switching with a single quantum dot coupled to a photonic crystal cavity, Phys. Rev. Lett. **108**, 227402 (2012).

[43] K. Kuruma, Y. Ota, M. Kakuda, S. Iwamoto, and Y. Arakawa, Time-resolved vacuum rabi oscillations in a quantum-dot–nanocavity system, Phys. Rev. B **97**, 235448 (2018).

[44] J.-H. Kim, C. J. K. Richardson, R. P. Leavitt, and E. Waks, Two-photon interference from the far-field emission of chip-integrated cavity-coupled emitters, Nano Letters **16**, 7061 (2016).

[45] Y. Sato, Y. Tanaka, J. Upham, Y. Takahashi, T. Asano, and S. Noda, Strong coupling between distant photonic nanocavities and its dynamic control, Nature Photonics **6**, 56 (2011).

[46] J. Schall, M. Deconinck, N. Bart, M. Florian, M. Helversen, C. Dangel, R. Schmidt, L. Bremer, F. Bopp, I. Hüllen, C. Gies, D. Reuter, A. D. Wieck, S. Rodt, J. J. Finley, F. Jahnke, A. Ludwig, and S. Reitzenstein, Bright electrically controllable quantum-dot-molecule devices fabricated by in situ electron-beam lithography, Advanced Quantum Technologies **4**, 2100002 (2021).

[47] P. M. Vora, A. S. Bracker, S. G. Carter, T. M. Sweeney, M. Kim, C. S. Kim, L. Yang, P. G. Brereton, S. E. Economou, and D. Gammon, Spin–cavity interactions between a quantum dot molecule and a photonic crystal cavity, Nature Communications **6**, 10.1038/ncomms8665 (2015).

[48] J.-H. Kim, S. Aghaeimeibodi, C. J. K. Richardson, R. P. Leavitt, and E. Waks, Super-radiant emission from quantum dots in a nanophotonic waveguide, Nano Letters **18**, 4734 (2018).

[49] M. Khoshnegar, T. Huber, A. Predojević, D. Dalacu, M. Prilmüller, J. Lapointe, X. Wu, P. Tamarat, B. Lounis, P. Poole, G. Weihs, and H. Majedi, A solid state source of photon triplets based on quantum dot molecules, Nature Communications **8**, 10.1038/ncomms15716 (2017).

[50] C. Carlson, D. Dalacu, C. Gustin, S. Haffouz, X. Wu, J. Lapointe, R. L. Williams, P. J. Poole, and S. Hughes, Theory and experiments of coherent photon coupling in semiconductor nanowire waveguides with quantum dot molecules, Phys. Rev. B **99**, 085311 (2019).

[51] S. Mukamel, Superoperator representation of nonlinear response: Unifying quantum field and mode coupling theories, Phys. Rev. E **68**, 021111 (2003).

[52] S. Mukamel, *Principles of Nonlinear Optical Spectroscopy*, Oxford series in optical and imaging sciences (Oxford University Press, 1995).

[53] H. Grabert, P. Schramm, and G.-L. Ingold, Quantum

brownian motion: The functional integral approach, Physics Reports **168**, 115 (1988).
[54] G. Vidal, Efficient classical simulation of slightly entangled quantum computations, Phys. Rev. Lett. **91**, 147902 (2003).
[55] See supplemental material at [url will be inserted by publisher] for (i) decomposition of tensors,(ii) green functions and model for the photonic crystal cavity system, (iii) dipole correlation function and localized detection, (iv) convergence analysis and consequences of approximate unitary.
[56] E. M. Stoudenmire and S. R. White, Itensor c++ library,http://itensor.org/, 2.1.0 and newer.
[57] M. Richter, K. J. Ahn, A. Knorr, A. Schliwa, D. Bimberg, M. E.-A. Madjet, and T. Renger, Theory of excitation transfer in coupled nanostructures – from quantum dots to light harvesting complexes, phys. stat. sol. (b) **243**, 2302 (2006).
[58] M. L. Kerfoot, A. O. Govorov, C. Czarnocki, D. Lu, Y. N. Gad, A. S. Bracker, D. Gammon, and M. Scheibner, Optophononics with coupled quantum dots, Nature communications **5**, 1 (2014).
[59] A. Zimmermann, S. Kuhn, and M. Richter, Poisson green's function method for increased computational efficiency in numerical calculations of coulomb coupling elements, Phys. Rev. B **93**, 035308 (2016).
[60] A. Nazir and D. P. McCutcheon, Modelling exciton–phonon interactions in optically driven quantum dots, J. Phys.: Cond. Matt. **28**, 103002 (2016).
[61] S. Lüker, K. Gawarecki, D. Reiter, A. Grodecka-Grad, V. M. Axt, P. Machnikowski, and T. Kuhn, Influence of acoustic phonons on the optical control of quantum dots driven by adiabatic rapid passage, Phys. Rev. B **85**, 121302 (2012).
[62] T. Renger and R. Marcus, On the relation of protein dynamics and exciton relaxation in pigment–protein complexes: an estimation of the spectral density and a theory for the calculation of optical spectra, J. Chem. Phys. **116**, 9997 (2002).
[63] R.-C. Ge and S. Hughes, Quantum dynamics of two quantum dots coupled through localized plasmons: An intuitive and accurate quantum optics approach using quasinormal modes, Phys. Rev. B **92**, 205420 (2015).
[64] S. Franke, S. Hughes, M. K. Dezfouli, P. T. Kristensen, K. Busch, A. Knorr, and M. Richter, Quantization of quasinormal modes for open cavities and plasmonic cavity quantum electrodynamics, Phys. Rev. Lett. **122**, 213901 (2019).
[65] P. Yao and S. Hughes, Macroscopic entanglement and violation of bell's inequalities between two spatially separated quantum dots in a planar photonic crystal system, Opt. Express **17**, 11505 (2009).
[66] Y. Yu, A. M. Delgoffe, A. Miranda, A. Lyasota, B. Dwir, A. Rudra, and E. Kapon, Remote excitation between quantum emitters mediated by an optical fano resonance, Optica **8**, 1605 (2021).
[67] H. T. Dung, L. Knöll, and D.-G. Welsch, Three-dimensional quantization of the electromagnetic field in dispersive and absorbing inhomogeneous dielectrics, Phys. Rev. A **57**, 3931 (1998).
[68] The maximum bond dimension of the MPS in all numerical calculations is truncated to below 200 and an accuracy of $\epsilon = 10^{-12}$, ΔT convergence is discussed in [55].
[69] L. Yang and S. Mukamel, Two-dimensional correlation spectroscopy of two-exciton resonances in semiconductor quantum wells, Phys. Rev. Lett. **100**, 057402 (2008).
[70] J. Kim, S. Mukamel, and G. D. Scholes, Two-dimensional electronic double-quantum coherence spectroscopy, Accounts of chemical research **42**, 1375 (2009).
[71] M. Richter, F. Schlosser, M. Schoth, S. Burger, F. Schmidt, A. Knorr, and S. Mukamel, Reconstruction of the wave functions of coupled nanoscopic emitters using a coherent optical technique, Phys. Rev. B **86**, 085308 (2012).
[72] F. Schlosser, A. Knorr, S. Mukamel, and M. Richter, Using localized double-quantum-coherence spectroscopy to reconstruct the two-exciton wave function of coupled quantum emitters, New Journal of Physics **15**, 025004 (2013).
[73] S. Hughes, Coupled-cavity qed using planar photonic crystals, Phys. Rev. Lett. **98**, 083603 (2007).
[74] M. Richter, Spatially localized spectroscopy for examining the internal structure of coupled nanostructures, physica status solidi (b) **250**, 1760 (2013), https://onlinelibrary.wiley.com/doi/pdf/10.1002/pssb.201200699.
[75] J. F. Specht and M. Richter, Reconstruction of exciton wave functions of coupled quantum emitters including spin with ultrafast spectroscopy using localized nanooptical fields, Applied Physics B **122**, 97 (2016).

Decomposition of tensors

Here, we will discuss the decomposition of $\tilde{M}$ and $\tilde{E}$ into products of lower dimensional tensors and the underlying ideas.

We start with $\tilde{M}$ and its decomposition:

$$\tilde{M}^{k'\alpha'_p\alpha'_s l'}_{psk\alpha_p\alpha_s l}(n) = \sum_{\substack{\tilde{s}_1\tilde{p}_1\\ \tilde{p}_2 m_2 m_t}} \tilde{M}^{(1),\alpha'_p}_{\tilde{p}_2,\alpha_p m_t m_2} \tilde{M}^{(2)k'\tilde{p}_2\alpha'_s l' m_t}_{\tilde{s}_1\tilde{p}_1 k\alpha_s m_2}(n) \tilde{M}^{(3)l'}_{m_2 m_t l} \tilde{M}^{(4)}_{\tilde{s}_1 s m_t} \tilde{M}^{(5)}_{\tilde{p}_1 p m_t} \tilde{M}^{(6)}_{s p m_t}. \tag{S1}$$

As seen in Eq. (5) the indices k and k' discriminate the different interactions handled in the tensor $\tilde{M}$. If k is not changed ($\delta_{k,k'}$) $\tilde{M}$ does not change anything and just passes the information through present in the indices α_p α_s, k and l, in this case the interaction, if any, happens in a subsequent tensor. If the index k is changed from 1 to -1 in k', the double time integrated correlation function in G describes a first system-bath interaction in the interval of the prior $\tilde{E}$ tensor, which is then finalized in the time interval connected to the $\tilde{M}$ tensor. Then the index l passes the information, if the system-bath interaction happened on the left or right side of the Liouville space in $\tilde{E}$ to the tensor $\tilde{M}$, whereas α_s and α_p pass information about the changed system Hilbert space states described in $\tilde{E}$ to the tensor $\tilde{M}$. Therefore α'_s and α'_p, which are passed to subsequent tensors $\tilde{M}$, are set to 1 (note we use indices for s and p starting with 1), which means the interaction already occurred and no subsequent interaction can occur on one of the remaining $\tilde{M}$.

The tensors used for the decomposition of $\tilde{M}$ reduce the number of indices per tensor and dimension of each of the indices. We start with $\tilde{M}^{(1)}$:

$$\tilde{M}^{(1),\alpha'_p}_{\tilde{p}_2,\alpha_p m_t m_2} = (\delta_{\alpha_p,\alpha'_p}\delta_{\tilde{p}_2,1}\delta_{m_t,3}\delta_{m_2,1} + \sum_{m_1=1,2} \delta_{m_2,1}\delta_{m_t,m_1}\delta_{\tilde{p}_2+1,\alpha_p}\delta_{\alpha'_p,1}). \tag{S2}$$

The value of the index m_t determines whether $\tilde{M}$ does not act on the system ($m_t = 3$) and thus just passes α_p through to α'_p, or whether α_p is passed via the index $\tilde{p}_2$ to the integrated correlation function G ($m_t = 1, 2$). m_1 indicates if the second interaction is on the left or right side and is passed to m_t. In the next tensor $\tilde{M}^{(2)}$, we include the double integrated correlation function G:

$$\begin{aligned}\tilde{M}^{(2),k',\tilde{p}_2,\alpha'_s l' m_t}_{\tilde{s}_1,\tilde{p}_1,k,\alpha_s m_2}(n) = \big(&\delta_{\alpha_s,\alpha'_s}\delta_{\tilde{s}_1,1}\delta_{\tilde{p}_1,1}\delta_{\tilde{p}_2,1}\delta_{m_2,1}\delta_{m_t,3}\delta_{k,k'} + \sum_{m_1=1,2}\sum_{\tilde{s}_2}\delta_{\tilde{s}_2+1,\alpha_s}\delta_{\alpha'_s,1}\delta_{m_t,m_1}\delta_{k',-1}\delta_{k,0}\\ &\cdot G_{\tilde{s}_1,\tilde{p}_1,\tilde{s}_2,\tilde{p}_2 m_1 m_2}(n)\big).\end{aligned} \tag{S3}$$

Again, for $m_t = 3$ the incoming α_s is just passed through to α'_s. Whereas for $m_t = m_1 = 1/2$ a second system bath interaction on the left/right side in Liouville space in G occurs. Therefore α_s is connected to G via the index $\tilde{s}_2$. G is included in $\tilde{M}^{(2)}$ and its other indices are passed to the other tensors in the product: $\tilde{p}_2$ to $\tilde{M}^{(1)}$, $\tilde{p}_1$ to $\tilde{M}^{(5)}$, $\tilde{s}_1$ to $\tilde{M}^{(4)}$, m_2 to $\tilde{M}^{(3)}$. The next tensor $\tilde{M}^{(3)}$ handles the distribution of the l index:

$$\tilde{M}^{(3)l'}_{m_2 m_t l} = \delta_{m2,1}\delta_{l,l'}\delta_{m_t,3} + \sum_{m_1=1,2}\delta_{m_1,m_t}\delta_{m_2+1,l}\delta_{l',1}. \tag{S4}$$

As usual, for $m_t = 3$, l is passed through to l', and for $m_t = m_1 = 1, 2$ l is passed to G. The next tensors starting with $\tilde{M}^{(4)}$ connect indices coming from G either with the left or right part of the indices s, p:

$$\tilde{M}^{(4)}_{\tilde{s}_1 s m_t} = \delta_{m_t,1}\delta_{s_L,\tilde{s}_1} - \delta_{m_t,2}\delta_{s_R,\tilde{s}_1} + \delta_{m_t,3}\delta_{\tilde{s}_1,1}, \tag{S5}$$

so for $m_t = 1$ $\tilde{s}_1$ is connected to s_L and for $m_t = 2$ $\tilde{s}_1$ is connected to s_R. $m_t = 3$ is the pass-through mode and effectively does nothing. $\tilde{M}^{(5)}$ is constructed in an analogous way:

$$\tilde{M}^{(5)}_{\tilde{p}_1 p m_t} = \delta_{m_t,1}\delta_{p_L,\tilde{p}_1} - \delta_{m_t,2}\delta_{p_R,\tilde{p}_1} + \delta_{m_t,3}\delta_{\tilde{p}_1,1}, \tag{S6}$$

since for $m_t = 1$ $\tilde{p}_1$ is connected to p_L and for $m_t = 2$ $\tilde{p}_1$ to p_R. The next tensor $\tilde{M}^{(6)}$ connects s and p either to the left or right part (on opposite site to the previous tensors!), and is controlled again by m_t:

$$\tilde{M}^{(6)}_{s p m_t} = \delta_{m_t,1}\delta_{s_R,p_R} + \delta_{m_t,2}\delta_{s_L,p_L} + \delta_{m_t,3}. \tag{S7}$$

Thus for $m_t = 3$ nothing happens, and for $m_t = 1$ the right sides of s and p are connected, whereas for $m_t = 2$ the left sides are connected.

Before we discuss the decomposition of $\tilde{E}$, we first discuss its contributions from Eq.(6): For $k = 0$ no interaction is happening in the interval ΔT, so we do not have to pass information to the $\tilde{M}$ tensors. On the other hand $k = -1$ means, so far nothing is applied to the time interval, the contribution will occur in one of the $\tilde{M}$, which are later added to interval ΔT, therefore $k = -1$ will not be included in the summation at the edge of network. Also $k = 2$ means no system bath interactions in subsequent $\tilde{M}$ inside ΔT, which are connected to other ΔT intervals. Finally for $k = 1$ one system-bath interactions occur in the ΔT interval associated with $\tilde{E}$, whereas the second occurs in another ΔT interval involving its $\tilde{M}$ tensor. Here l encodes the side of the Liouville space (left or right), on which the system bath interaction occurs.

Again the tensors used for the decomposition of $\tilde{E}$ into low rank and dimensional tensors read:

$$\tilde{E}^{\alpha_p,\alpha_s l}_{s,p,k} = \sum_{m_1 m_2 q_1 q_2 s_1 p_2} E^{(1)}_{p_L s_L k m_1 m_2} E^{(2)}_{p_R s_R k m_1 m_2} E^{(3)}_{p_L p_R q_1 q_2} E^{(4)}_{s_L s_R m_1 m_2 q_2} E^{(5)}_{m_1 m_2 s_1 q_1 q_2 p_2 l} E^{(6)}_{s_L s_R \alpha_s s_1 m_1 m_2} E^{(7)}_{p_L p_R \alpha_p p_2 m_1 m_2}, \tag{S8}$$

which reduces the number and dimension of the used indices, and thus made the numerical calculations more feasible.

The first tensor, $E^{(1)}$, in the product

$$E^{(1)}_{p_L s_L k m_1 m_2} = \delta_{k,0}\delta_{p_L,s_L}\delta_{m_1,1}\delta_{m_2,1} + \delta_{k,-1} + \delta_{k,2}(1 - \delta_{m_1,2}\delta_{m_2,2}) + \delta_{k,2}\delta_{m_1,2}\delta_{m_2,2}\delta_{p_L,s_L} + \delta_{k,1}(\delta_{m_2,1} - \delta_{m_2,2}\delta_{p_L,s_L}), \tag{S9}$$

connects the left part p_L and s_L, if no system-bath interaction in ΔT occurs ($k = 0$), if two interactions at the left side occur ($k = 2$ with $m_1 = 2$ and $m_2 = 2$) or if one interaction on the right side takes place ($k = 1$ with $m_2 = 1$). The second tensor $E^{(2)}$:

$$E^{(2)}_{p_R s_R k m_1 m_2} = \delta_{k,0}\delta_{p_R,s_R}\delta_{m_1,1}\delta_{m_2,1} + \delta_{k,-1} + \delta_{k,2}(1 - \delta_{m_1,1}\delta_{m_2,1}) \quad + \delta_{k,2}\delta_{m_1,1}\delta_{m_2,1}\delta_{p_R,s_R} + \delta_{k,1}(\delta_{m_2,1}\delta_{p_R,s_R} + \delta_{m_2,2}) \tag{S10}$$

works in the same way, only that it acts on the right side instead of the left side, thus right and left (also encoded in 1 and 2 for m_1 and m_2) is exchanged and a sign difference caused by the commutator. The term, $E^{(3)}$, is only important for two system bath interaction per ΔT

$$E^{(3)}_{p_L p_R q_1 q_2} = (\delta_{k,0} + \delta_{k,-1} + \delta_{k,1})\delta_{q_1,1}\delta_{q_2,1} + \delta_{k,2}(\delta_{m_1 m_2}\delta_{q_1,q_2} + \delta_{m_1,1}\delta_{m_2,2}\delta_{q_1,p_L} + \delta_{m_1,2}\delta_{m_2,1}\delta_{q_1,p_R}), \tag{S11}$$

and only for $k = 2$ is something done. It either connects the indices q_1 q_2 of the correlation function G, if the first and second system-bath interaction occurs both on the left or on the right side, or q_1 is connected either to the left or right side of p, these contributions are a result of the double commutator of the system bath coupling. The next factor $E^{(4)}$ completes the work for the correlation function G:

$$E^{(4)}_{s_L s_R m_1 m_2 q_2} = \big(\delta_{k,0} + \delta_{k,-1} + \delta_{k,1}\big)\delta_{q_2,1}\delta_{m_1,1}\delta_{m_2,1} - \delta_{m_1,2}\delta_{m_2,1}\delta_{q_2,s_L} + \delta_{m_1,m_2}) \tag{S12}$$

and connects for $k = 2$ with interaction on left and right the index q_2 either to the left or right side of s. The next factor $E^{(5)}$ serves two purposes:

$$E^{(5)}_{m_1 m_2 s_1 q_1 q_2 p_2 l} = ((\delta_{k,0} + \delta_{k,-1})\delta_{m_2,1}\delta_{l,1} + \delta_{k,1}\delta_{m_2,l+1}) - \delta_{k,2}\delta_{l,1}G_{s_1,q_1,q_2,p_2,m_1,m_2}, \tag{S13}$$

which contains the double integrated correlation function G for the two interaction in ΔT (case $k = 2$) and for $k = 1$ it connects l shifted by one to m_2 to pass it on to the M tensors. The indices q_1 and q_2 are passed to G from the previous tensors, where as s_1 and p_2 will come from the proceeding tensors, starting with $E^{(6)}$:

$$\begin{aligned} E^{(6)}_{s_L s_R \alpha_s s_1 m_1 m_2} =& (\delta_{k,0} + \delta_{k,-1})\delta_{\alpha_s,1}\delta_{m_1,1}\delta_{m_2,1}\delta_{s_1,1} + \delta_{k,2}\delta_{\alpha_s,1}(\delta_{m_1,1}\delta_{s_1,s_L} + \delta_{m_1,2}\delta_{s_1,s_R}) \\ &+ \delta_{k,1}\delta_{m_1,1}(\delta_{m_2,1}\delta_{s_L,\alpha_s+1}\delta_{s_1,1} + \delta_{m_2,2}\delta_{s_R,\alpha_s+1}\delta_{s_1,1}), \end{aligned} \tag{S14}$$

where for $k = 2$, s_1 is depending on m_1 either to the left or right side of s. For $k = 1$ the left or right side of s (depending on m_2) is connected to α_s shifted by 1, to connect it to a $\tilde{M}$ tensor for the second system-bath interaction. The last factor $E^{(7)}$ works in a similar way:

$$\begin{aligned} E^{(7)}_{p_L p_R \alpha_p p_2 m_1 m_2} =& (\delta_{k,0} + \delta_{k,-1})\delta_{\alpha_s,1}\delta_{m_1,1}\delta_{m_2,1}\delta_{s_1,1} + \delta_{k,2}\delta_{\alpha_p,1}(\delta_{m_2,1}\delta_{p_2,p_L} + \delta_{m_2,2}\delta_{p_2,p_R}) \\ &+ \delta_{k,1}\delta_{m_1,1}(\delta_{m_2,1}\delta_{p_L,\alpha_p+1}\delta_{p_2,1} + \delta_{m_2,2}\delta_{p_R,\alpha_p+1}\delta_{p_2,1}), \end{aligned} \tag{S15}$$

for $k = 2$ it connects either the left or right side (depending on m_2) of p to p_2 for passing it to the correlation function g. For $k = 1$ the left or right side of p is passed to α_p shifted by 1.

Green functions and model for the photonic crystal cavity system

The electromagnetic response functions can be defined in terms of the photonic Green functions, defined from

$$\boldsymbol{\nabla}\times\boldsymbol{\nabla}\times\mathbf{G}(\mathbf{r},\mathbf{r}',\omega)-\frac{\omega^2}{c^2}\epsilon(\mathbf{r},\omega)\mathbf{G}(\mathbf{r},\mathbf{r}',\omega)=\mathbb{1}\delta(\mathbf{r}-\mathbf{r}'), \tag{S16}$$

with suitable boundary conditions. Following the approach of Refs. 65 and 73, these can be obtained in an analytical form using mode expansion techniques and exploiting the completeness relation of the Green function, and we consider the two cavity modes and the waveguides modes as the only modes of interest in the problem. We assume identical cavities, that are side-coupled to a waveguide mode, and separated by a distance L; we also consider a TLS embedded in each cavity at a field antinode position, aligned with the polarization of the cavity mode. Subsequently, the correlation functions, defined from $G_{nm}(\omega)=\mathbf{d}_{12}^{(n)}\cdot\mathrm{Im}(\mathbf{G}(\mathbf{r}_1,\mathbf{r}_1,\omega))\cdot\mathbf{d}_{12}^{*(m)}$, take the form [65]

$$G_{11}(\omega)=\frac{\omega^2E_1E_1}{\omega_c^2-\omega^2-i\omega\gamma_c(1+e^{i2\phi}R_2(\omega))-i\omega\gamma_0}, \tag{S17}$$

$$G_{22}(\omega)=\frac{\omega^2E_2E_2}{\omega_c^2-\omega^2-i\omega\gamma_c(1+e^{i2\phi}R_1(\omega))-i\omega\gamma_0}, \tag{S18}$$

$$G_{12}(\omega)=\frac{\omega^2R_1(\omega)e^{i\phi}E_1E_2}{\omega_c^2-\omega^2-i\omega\gamma_c(1+e^{i2\phi}R_1(\omega))-i\omega\gamma_0}, \tag{S19}$$

$$G_{21}(\omega)=\frac{\omega^2R_2(\omega)e^{i\phi}E_1E_2}{\omega_c^2-\omega^2-i\omega\gamma_c(1+e^{i2\phi}R_2(\omega))-i\omega\gamma_0} \tag{S20}$$

with $E_{1/2}=\frac{1}{\epsilon_rV_{\text{eff}}}$ (with V_{eff} the effective mode volume and ϵ_r the dielectric constant of the photonic crystal slab), $R_1(\omega)=R_2(\omega)=\frac{i\omega\gamma_c}{\omega_c^2-\omega^2-i\omega(\gamma_c+\gamma_0)}$, and $\gamma_c=Q_c/\omega_c$. The cavity decay rates include on-chip decay from the cavity to the waveguide, γ_c, as well as off-chip decay, γ_0, where the latter is typically much smaller than the former (to maintain a waveguide mode beta factor). The round trip phase is determined from $2\phi=2k_BL+\varphi$, $k_B=\omega n_g/c$ and we set $\varphi=0.8\pi$.

Parameters used in the main text (if not others specified): $\epsilon_r=12$, $L=2\lambda$ (waveguide length in wavelengths) $n_g=10$ (group velocity index), $\omega_c=200$THz frequency of the cavities, $Q_c=2000$ quality factor of the cavity, $V_{\text{eff}}=5\cdot10^7\text{nm}^3$ mode volume, $\varphi=0.8\pi$ out of plane loss 1% of cavity loss ($\gamma_0=0.01\gamma_c$).

Dipole correlation function and localized detection

The single quantum $\langle P(t)P^\dagger(0)\rangle$ and double quantum dipole correlation function $\langle P(t)P(t)P^\dagger(0)P^\dagger(0)\rangle$ allow a direct inspection of the system eigenenergies, and spectral resonances, for one or two excitations in the system, if the system is initially in the ground state. For example, $\langle P(t)P^\dagger(0)\rangle$ describes a coherence between the ground state and single excited states created by polarisation flip operator $P^\dagger(0)$ at time 0 and inspected at time t by $P(t)$. Thus by varying t, the coherent oscillation can be scanned, and its Fourier transform corresponds to the linear optical response and we can deduce from the individual resonances the bright single excited states of system.

On the other hand, for $\langle P(t)P(t)P^\dagger(0)P^\dagger(0)\rangle$ at time 0, $P^\dagger(0)P^\dagger(0)$ described the coherence between the ground state and double excited states; similar to the linear, single excitation case, the double excited states can be scanned and a Fourier transform retrieves the energies of the double excited states available for two photon excitation. As in the linear case, experimental techniques exist to access this correlation function [70].

However, for the example system in the main Letter, the situation is a bit different to the usual experimental situation, since we include only polarization operators of the quantum emitters, for the operators $P^\dagger$. But in the system, the coupling to the photons can be strong, so that eigenstates are in fact polariton states, that also include a photon mode part. Assuming photon mode operators $b_j^\dagger$, then the single excitation eigenstates $|e\rangle$ are a superposition state,

$$|e\rangle=c_e^1\sigma_1^\dagger|0\rangle+c_e^2\sigma_2^\dagger|0\rangle+\sum_j c_e^{pj}b_j^\dagger, \tag{S21}$$

with $\sigma_l^\dagger=|2\rangle_l\langle1|_l$ and an overall ground state $|0\rangle$. So it is clear that we miss the photon part in the spectra. In an analogues way, the double excited eigenstates $|f\rangle$ can be expanded in the local states.

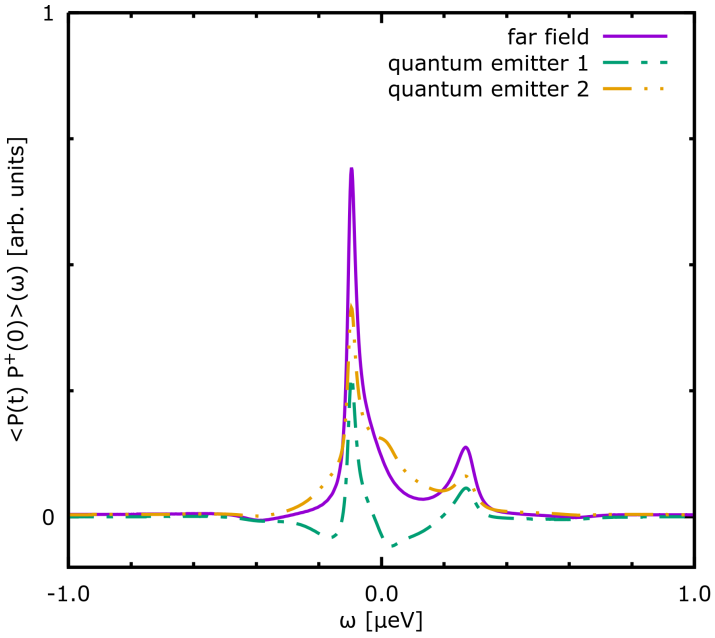


Figure S1. Dipole correlation function $\langle P(t)P^\dagger(0)\rangle$ for a system initially on an excited density at emitter 1 for far field detection (detection in $P(t)$ contains both emitters) and for localized detection at the quantum emitter (detection in $P(t)$ contains only one emitter).

In an experimental pump probe experiment, the pulses are also only acting on the quantum emitters and are much faster compared to the transfer process to the photon modes, thus that local densities $|2\rangle_l\langle 2|_l$ are prepared in the excited system. We can access this contribution also by inspecting $\langle P(t)P^\dagger(0)\rangle$ for a system where the first quantum emitter is initially in the local excited state. Of course this is not an eigenstate of the system but a superposition of $|e\rangle$, furthermore after the polarisation operator at t the system is in a coherence between states $|f\rangle$ and $|e\rangle$, creating the second excitation in the other emitter. We see in Fig. S1 precisely the same features as in the nonlinear signal in the main text. The negative features are of course puzzling, but can be a result, that the system is in the local basis and thus expansion coefficients such as c_e^1 or c_f^{12} etc, and their phase enter the signal. While our method does not allow to access the bath—the photon part—we can show, that if we detect only one quantum emitter [71, 72, 74, 75], formally dark state can give negative contributions in the spectrum (cf. Fig. S1) and likely this is also the case for the negative contributions with respect to the photon part.

Convergence analysis and consequences of approximate unitary

Main parameters for the numerically convergence are the truncation bond dimensions and accuracy for the tensor network and the quantum path integral time discretization ΔT.

For truncating bonds the MPS after MPO application, we use a maximum bond dimension as well as a accuracy for determining the truncated dimension. This is necessary since the different layers of the network within a time step have quite different bond dimensions (one order magnitude possible). So for some of them bond dimension is the best parameter to do the truncation and for the others accuracy is the best for keeping the important information in the network. This is at least our subjective experience while designing the algorithm. Some intermediate layers require relative low bond dimension. There relative useless information for the next will be included without an accuracy truncation parameter. This will prevent a fast calculation in subsequent layers, which require higher bond dimensions cause by the additional useless information. Even worse, it could prevent convergence at all.

The time propagation U_i over an interval ΔT is expanded in Eq. (1) in orders of the system-bath interaction, thus it is only $O(\Delta t^2)$ unitary. In principle this can have consequences on semi-positivity and trace preservation of the reduced density matrix thus the density matrix elements over time as plotted in Fig. 5 d).

In fact, if we choose a ΔT, which is too large, we see large negative values e.g. for the reduced density of the double excited state matrix ρ_{2222} as shown in Fig. S2, but these problems disappear for sufficiently small ΔT. Problems

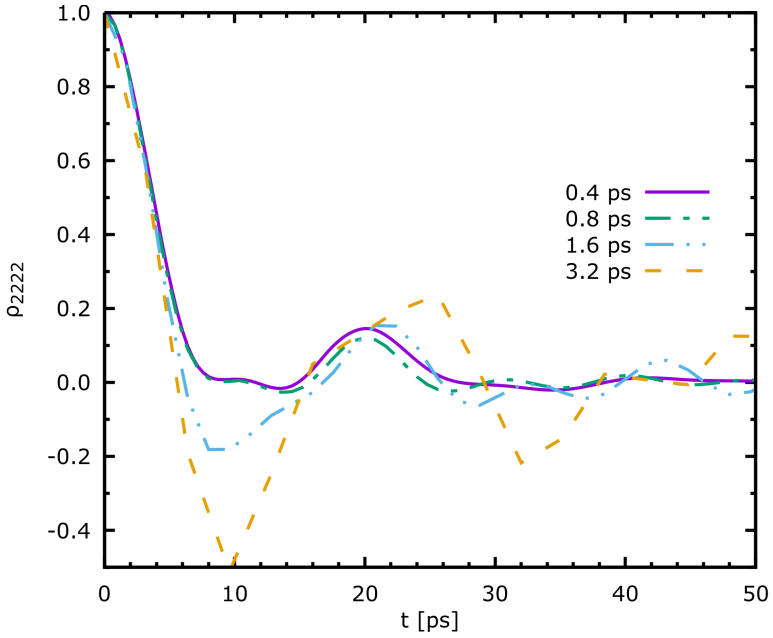


Figure S2. Reduced density matrix element ρ_{2222} for the example from Fig. 5 d) for different discretizations Δt of the quantum path integral.

with violation of density matrix positivity also occur if too strong truncation removes two many quantum path ways. The violated positivity in ρ_{2222} can also be seen in the numerical calculation used for Fig. 5(a), but it occurs after the polarizations are created, so it can not be the origin of the negative signatures, since only secular terms are included in the system bath coupling, which do not convert polarizations into densities and vice versa. Therefore the densities are completely decoupled from the plotted observables.